

# Circuit Folding: Modular and Qubit-Level Workload Management in Quantum-Classical Systems

Shuwen Kan  
Fordham University  
New York, NY, USA

Yanni Li  
Fordham University  
New York, NY, USA

Hao Wang  
Stevens Institute of Technology  
Hoboken, NJ, USA

Sara Mouradian  
University of Washington  
Seattle, WA, USA

Ying Mao  
Fordham University  
New York, NY, USA

## Abstract

Quantum computing is an emerging technology that offers exponential speedups for certain problems. At the core of quantum-centric supercomputing is advanced middleware that manages the interaction between quantum hardware and classical computing infrastructure. Circuit knitting is a technique that leverages classical computation to offload some of the computational burden from quantum circuits, enabling them to exceed the capacity of current Noisy Intermediate-Scale Quantum (NISQ) devices. This is done by partitioning large circuits into smaller subcircuits, though at the cost of classical reconstruction and increased sampling overhead. Despite significant advancements in reducing the theoretical costs of circuit knitting, efficiently deploying these techniques across a broad range of quantum algorithms remains a challenge. In this work, we propose CiFold, a novel graph-based system that, at individual qubit’s level, identifies and leverages repeated structures within quantum circuits. By folding these repeated modules in parallel, CiFold constructs a meta-graph that guides the partitioning process, optimizing the cutting strategy through the integration of advanced circuit knitting techniques. Our system has been extensively evaluated across various quantum algorithms, achieving up to 799.2% reduction in quantum resource usage, demonstrating its scalability and substantial performance improvements over state-of-the-art approaches.

---

Corresponding authors: {sk107, ymao41}@fordham.edu.

---

Permission to make digital or hard copies of all or part of this work for personal or classroom use is granted without fee provided that copies are not made or distributed for profit or commercial advantage and that copies bear this notice and the full citation on the first page. Copyrights for components of this work owned by others than the author(s) must be honored. Abstracting with credit is permitted. To copy otherwise, or republish, to post on servers or to redistribute to lists, requires prior specific permission and/or a fee. Request permissions from [permissions@acm.org](mailto:permissions@acm.org). *Conference’25, March 2025, Rotterdam, The Netherlands*

© Copyright held by the owner/author(s). Publication rights licensed to ACM.

ACM ISBN 978-x-xxxx-xxxx-x/YY/MM

## ACM Reference Format:

Shuwen Kan, Yanni Li, Hao Wang, Sara Mouradian, and Ying Mao. . Circuit Folding: Modular and Qubit-Level Workload Management in Quantum-Classical Systems. In . ACM, New York, NY, USA, 15 pages.

## 1 Introduction

Quantum computing holds immense potential to revolutionize various fields by solving complex problems currently intractable for classical computers, such as cybersecurity [18, 30, 41, 58], machine learning [13, 22, 25, 31, 40, 50–53, 57, 59], chemical simulation [16, 39], databases and system design [26, 27, 46, 47, 60]. For example, in drug discovery [33, 34, 61], quantum computers can simulate molecular interactions at the quantum level with unprecedented accuracy. However, the current era of quantum computing, known as the Noisy Intermediate-Scale Quantum (NISQ) era, presents significant challenges. Firstly, despite advances in various qubit architectures, such as superconducting qubits, neutral atoms, trapped ions, and photons, existing quantum computers have limited qubit counts, typically around 50-150. These limited on-board resources significantly restrict practical applications. Additionally, inherent noise in physical qubits makes quantum algorithms error-prone and leads to low algorithmic fidelity issues [2]. While quantum error correction and mitigation are under intensive study, they suffer from scalability problems, as the effects of noise grow exponentially with the number of qubits. Therefore, in addition to designing fault-tolerant algorithms, it is equally important to develop approaches that execute large circuits on existing quantum hardware.

To leverage the smaller-size quantum hardware, circuit cutting techniques, such as CutQC [54], FitCut [28], and CKT [5], have emerged as effective strategies. Given a quantum-classical system equips with both quantum and classical resources, these techniques aim to cut large quantum circuits into smaller subcircuits that can be executed on current quantum hardware. Quantum circuit cutting typically involves two phases, cut point finding and subcircuit reconstruction. Both phases run on the classical resources, e.g., CPUs and GPUs. In the first phase, the circuit is analyzed to identify optimal cutting points where the circuit can be split into

smaller subcircuits. These points are chosen to minimize the computational overhead while preserving the accuracy of the overall computation. In the second phase, after executing the subcircuits independently, a classical post-processing step is used for reconstruction, where the results from the subcircuits are combined using techniques like tensor networks or probabilistic methods to recover the original circuit's output with minimal error. However, existing circuit-cutting solutions suffer from large overheads in both phases and require large amount of quantum executions. [48] introduced methods such as parallel cutting that attempt to balance cutting efficiency and resource usage. However, one key limitation is that the cutting points must be predefined and known in advance. With the increasing diversity of quantum circuits, a static approach becomes impractical. As quantum circuits grow more complex, automatically identifying optimal cutting points becomes crucial, and current methods fall short of addressing these higher-level requirements.

In this project, we propose CiFold, a system designed to reduce overhead in both cutting point identification and subcircuit execution. Theoretically, CiFold adopts a circuit knitting technique, an effective approach that not only reduces the overhead associated with circuit cutting but also improves fidelity. Additionally, CiFold dynamically identifies optimal cutting points, eliminating the need for predefined locations and adapting to the complexity and diversity of quantum circuits. CiFold decomposes a circuit down to the individual qubit level, aiming to identify modules with repeated patterns. These identified modules can be folded across different qubits, further optimizing the circuit. By addressing inherent noise and complexity issues, CiFold ensures scalability, making it a practical solution for large-scale quantum computations. Our system offers several key contributions and improvements:

- CiFold introduces a graph-based framework for qubit-level circuit management in quantum-classical systems. By modeling quantum circuits as graphs and folding them at the qubit level, CiFold identifies recurring patterns (i.e., gate sets) across different circuit fragments, thereby reducing overall complexity.
- CiFold efficiently searches for optimal partitioning and adapts to the limited quantum resources available. By reusing outputs across multiple foldable modules, CiFold reduces the number of subcircuit executions.
- We propose Quantum Resource Overhead (QRO), a new metric that accounts for the number of cuts, subcircuit variations, subcircuit executions, and their widths and depths. QRO effectively quantifies the additional quantum resources required due to circuit cutting.
- We implemented CiFold using IBM Qiskit and conducted extensive experiments on various types of circuits with different qubit constraints and sizes. The results demonstrate that CiFold improves the accuracy

of observable values in noisy executions and significantly reduces Quantum Resource Overhead—by up to 799.2% compared to other state-of-the-art methods—while maintaining an ultra-fast cut point identification process.

## 2 Related Work

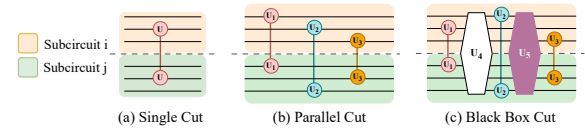


**Figure 1.** Three types of cuts: in black box cut, parallel cuts are blocked by unknown, irrelevant operations

The hybrid quantum-classical approach has become crucial in the NISQ era, as quantum computers alone often fail to deliver reliable results. Circuit knitting for decomposition, which allows the execution of circuits beyond current hardware limitations by splitting them into smaller fragments, has been actively studied. However, this technique introduces exponential overhead in both classical reconstruction and quantum execution, leading to ongoing research to mitigate these costs. Recent work [48] categorizes gate cuts into three types: single cut (Figure 1(a)), parallel cut (Figure 1(b)), and blackbox cut (Figure 1(c)), where cuts are separated by unknown operations. It has been shown that parallel cutting, rather than multiplying overhead for each cut, significantly reduces costs, even in blackbox cases with two ancilla qubits.

Previous studies [7, 44] show that classical communication between subcircuits can further lower overhead, reducing it from  $16^n$  to  $(2^{(n+1)} + 1)^2$  for  $n$  parallel wire cuts. Traditional wire cutting relies on inserting measure-and-prepare channels at cutting points [43], though methods like randomized insertion [35] add the cost of one ancilla qubit per cut. To address this, ancilla-free wire decomposition methods [23, 42] reduce qubit requirements, making hardware implementation more feasible. Other research [8, 9] focuses on optimizing classical reconstruction, with sampling-based postprocessing to reduce computational overhead.

Different implementations of circuit cutting have demonstrated improved accuracy in the results compared to executing the original circuit on a higher-qubit-count computer [3]. [17] discussed the use of circuit cutting on variational quantum algorithm. When combined with advancements in underlying hardware, these implementations validate the effectiveness of circuit cutting in achieving high-accuracy executions of large-width circuits. There are ongoing efforts within the industry to develop circuit-cutting pipelines that enable automated detection of cutting points and establish unified cut operations compatible with various compilers. An example of such software is `qiskit-addon-cutting`, which integrates multiple circuit cutting techniques [5].

Apart from existing literature, CiFold aims to reduce overhead by identifying modules with repeated patterns at the individual qubit level. These modules can be folded and processed in parallel. CiFold constructs a meta-graph to guide the partitioning process, optimizing the cutting strategy through the integration of circuit knitting techniques.

### 3 Background and Motivation

This section introduces the background of quantum computing and circuit management in a quantum-classical system.

#### 3.1 Quantum Circuits in Quantum-Classical Systems

A quantum circuit is a computational model that applies a sequence of quantum gates to a set of qubits, analogous to classical logic gates but operating on quantum states. Each gate manipulates the quantum state of one or more qubits. For example, the Hadamard gate (H) creates superposition by transforming a qubit's state from  $|0\rangle$  or  $|1\rangle$  to a linear combination of both states. The CX gate (CNOT) is a two-qubit gate that flips the state of the target qubit if the control qubit is in state  $|1\rangle$ . Quantum circuits are typically represented visually, with qubits shown as horizontal lines and gates placed along these lines in the order they are applied. The circuit ends with measurement gates that collapse the qubits' superposition into classical values. By combining multiple quantum gates, circuits perform complex quantum computations that leverage superposition, entanglement, and interference.

However, in the current Noisy Intermediate-Scale Quantum (NISQ) era, quantum hardware is constrained by limited qubit counts and various noises, making running large-scale quantum algorithms challenging. To address this, quantum-classical systems are utilized, integrating both quantum and classical computing resources. Quantum processor units (QPUs) perform operations that take advantage of quantum mechanics, while classical processors (e.g., CPUs/GPUs) handle tasks like optimization, error correction, circuit cutting, and result reconstruction. This hybrid approach is essential for making current quantum devices more practical and effective, enabling progress in fields like machine learning, chemistry, and cryptography, where a combination of quantum and classical resources is necessary for near-term solutions.

#### 3.2 Quantum-Classical Workload Management

To maximize the capabilities of current quantum hardware with limited qubit counts, quantum-classical systems typically handle three types of workloads: (1) Cut Point Finding—identifying specific points to divide large quantum circuits into smaller, manageable subcircuits, (2) Subcircuit Execution—running the subcircuits multiple times with varying initial states, and (3) Result Reconstruction—combining the results from individual subcircuits to recreate the outcome of

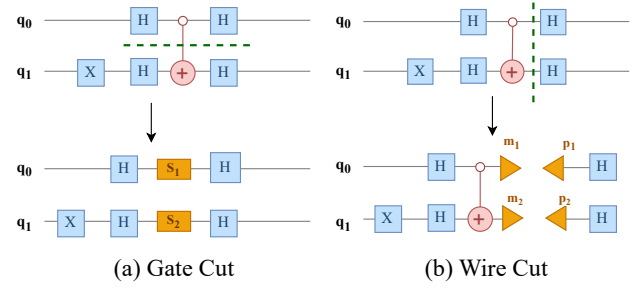


Figure 2. Two cut types: gate cut and wire cut.

the original circuit. Types 1 and 3 are performed by classical parts, while Type 2 involves quantum processing.

**3.2.1 Cutting Point Finding.** Circuit Cutting aims at decomposing large quantum circuits into smaller subcircuits that are compatible with current quantum hardware. Additionally, it helps in reducing circuit depth and width, thereby mitigating computational errors and improving the overall fidelity. Circuit cutting developed based on the idea of Quasiprobability Simulation [24]. Upon cutting large quantum circuits into smaller ones, the connections between both sides of the cutting points should be replaced into simpler operations which can be done through Quasiprobability Simulation. There are two main techniques of cutting point finding: Gate Cut and Wire Cut.

**Gate cut:** In a *space-like (gate) cut*, two-qubit gates are replaced by a sequence of single-qubit operations and classical post-processing steps. The two-qubit gates can then be simulated by 1 qubit gate operations on each qubit independently [36]. In the Figure 2(a),  $S_1$  and  $S_2$  denote the independent single-qubit operations which replace the two-qubit gate.

**Wire cuts:** In a *time-like (wire) cut*, the identity channel representing a quantum wire is replaced by measurements and preparations. As illustrated in Figure 2(b), when two wires are cut,  $m_1$  and  $m_2$  denote the extra measurements while  $p_1$  and  $p_2$  represents the initial state preparations for a separate computation fragment.

**3.2.2 Subcircuit Execution.** Existing quantum hardware inherently provide probabilistic measurement outcomes, making sampling necessary when large circuits are cut into smaller subcircuits. Since each subcircuit execution yields only partial information, repeated executions are required to accurately estimate the full distribution of outcomes [54]. The sampling overhead for each pair of subcircuits can be formulated as:

$$\text{Sampling Overhead} = \gamma_{ij}^n, \quad (1)$$

where  $\gamma_{ij}$  represents the sampling product factor between each pair of subcircuits  $i$  and  $j$ , and  $n$  denotes the number of cutting points between them. For instance, if there is only one cutting point between subcircuit  $i$  and  $j$ , the sampling

overhead is simply  $\gamma_{ij}$ . However, if there are ten cutting points between these subcircuits, the sampling cost becomes  $\gamma_{ij}^{10}$ , which increases exponentially with the number of cuts.

**3.2.3 Result Reconstruction.** During reconstruction phase, the output states from each subcircuit must be combined to reproduce the final computational outcome of the entire quantum circuit. This step involves computing multiple combinations of measurement results from subcircuits [54]. The reconstruction overhead is multiplicatively increased for multiple cuts.

### 3.3 Motivation: Qubit-level Repeated Patterns

Existing circuit cutting techniques face significant computational overhead in both the cutting and reconstruction phases. As the number of qubits in the input circuit increases, the number of required subcircuit executions and reconstructions quickly becomes infeasible on real quantum hardware, making current approaches unscalable. This challenge inspired the development of CiFold, which aims to maintain comparable algorithmic fidelity to existing methods while significantly reducing and controlling the computational cost.

CiFold is based on the insight that in a quantum-classical system, workloads (i.e., circuits) can be characterized at the individual qubit level. From the perspective of a single qubit, operations include single-qubit gates, such as the Hadamard (H) gate and X gate, which affect only that qubit, as well as multi-qubit gates, such as the Controlled-NOT (CNOT) gate, which involve multiple qubits. When analyzing workloads across multiple qubits, repeated patterns of gate sequences often emerge. If subcircuits contain identical patterns, the system can treat them as a single subcircuit with multiple instances, reducing execution redundancy.

Figure 3 illustrates sample circuits from four quantum algorithms: Bernstein-Vazirani (BV)[4], Quantum Fourier Transform (QFT)[10], Hardware-Efficient Ansatz (HWEA)[29], and Grover’s Search Algorithm[20]. Repeated patterns, highlighted by the green and red boxes at the qubit level, can be observed in all these circuits. For example, in the BV algorithm, from  $q_0$ ’s perspective, there is a Hadamard gate, followed by a CNOT gate between  $q_0$  and  $q_2$ , and ending with another Hadamard gate. Similarly,  $q_1$  follows the same pattern, with a Hadamard gate, a CNOT gate, and a final Hadamard gate. In this case, the same sequence of three gates appears on both qubits. Similar patterns are found across the other algorithms such as stabilizer circuit in quantum error correction[56] with different gate sequences and pattern sizes.

Based on this insight, our system decomposes the input circuit’s workload at the qubit level. It identifies the largest modules, i.e., repeated patterns, for each qubit and “folds” multiple identical modules together. This allows the system to treat them as a single unit during subcircuit execution

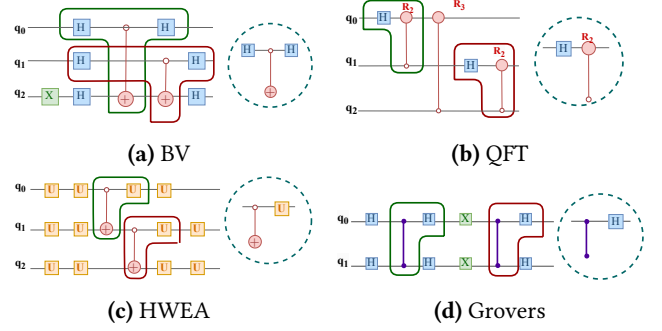


**Figure 3.** Four sample circuits with repeated patterns: (a) Bernstein Vazirani (BV); (b) Quantum Fourier Transform (QFT); (c) Hardware efficient ansatz (HWEA) and (d) Grover’s Search Algorithm (Grovers).

and final result reconstruction, significantly optimizing the process.

## 4 Problem Formulation

In this section, we present our problem formulation and our optimization objectives.

QuasiProbability simulation [55] is a method of simulating a linear operation  $\mathcal{E}$  via a set of available operations  $\mathcal{S}$  that can be physically realized. QuasiProbability Decomposition (QPD) method is primarily used for error mitigation [14, 15, 55] by simulating a noise-free quantum operation with noisy operations couple with strategically post-processing the samples. Concretely, we can simulate an two-qubit gate  $\mathcal{E}$  if we can decompose it as

$$\mathcal{E} = \sum_{i=1}^m a_i \mathcal{F}_i, \quad \gamma = \left( \sum_i |a_i| \right)^2, \quad (2)$$

where:

- $\mathcal{F}_i$  is local operations on a single qubit and  $a_i$  is the corresponding coefficient.
- $m$  is the total number of different local operations needed.
- $\gamma$  is the sampling overhead for this QuasiProbability distribution simulation. In the case of multiple QPD exist, the sampling overhead is multiplicative.

In QPD’s application on circuit knitting[37, 38], the number of samples is lower bounded by a desired error  $\gamma^{2n} \cdot \frac{1}{\epsilon^2}$  [55].  $\gamma$  is different across different types of operations to be decomposed. For example, the CNOT gate family has a  $\gamma^2$  of 9, whereas the SWAP gate, known as most expensive two-qubit gate to cut has a  $\gamma^2$  of 49. Due to the multiplicative nature of  $\gamma$ , finding an optimal decomposition with the lowest  $\gamma$  for each type of operations is crucial. This is an active research area with many works proposing different optimal

decomposition, cutting protocols, and techniques like introducing classical communication between local operations or utilizing ancilla qubits.

Under the CiFold framework, we aim to reduce the quantum resource cost from each individual qubit's level while maintaining optimal classical cost. We employ a graph-based approach to identify the repeated module of input circuit and find an optimal partitioning with the consideration of qubit constraints on the quantum machines. For a quantum circuit  $C$  partitioned into  $n$  subcircuits,  $\{c_1, \dots, c_n\} \subseteq C$ . We define the quantum resource overhead (QRO) to be:

$$\text{QRO} = \sum_{i=1}^n \left( \prod_{j \in s_i} \gamma_{ij} \times w(c_i) \times d(c_i) \right), \quad (3)$$

where:

- $s_i$ : The set of cuts between subcircuit  $i$  and the other subcircuits.
- $\gamma_{ij}$ : The  $\gamma$ -factor of the cut between subcircuit  $i$  and subcircuit  $j$ .
- $\prod_{j \in C_i} \gamma_{ij}$ : The variations of subcircuits when replacing the original quantum channel with multiple types of local operations.
- $w(c_i)$  and  $d(c_i)$ : The *width* and *depth* of subcircuit  $i$ , where  $w(c_i)$  denotes the number of qubits in  $c_i$  and  $d(c_i)$  denotes the number of layers of quantum gates in  $c_i$ .

The product of circuit width ( $w$ ) and depth ( $d$ ) in QRO is defined retroactively based on the concept of quantum volume, which measures the product of width and depth that can be reliably executed on a quantum processing unit (QPU). Therefore, we define  $w \times d$  as a counterpart for quantum circuits, where both the circuit width and depth contribute to the quantum resource requirements (i.e., how powerful the QPU must be to execute it reliably). For very large quantum circuits, even if they fit on a quantum computer, they may not be reliably executed, meaning that if you fully utilize all the qubits, the resulting circuit would be highly unreliable.

Another underlying assumption for building the cost function is that a fixed expected error, denoted as  $\epsilon$ , is maintained for all cuts introduced during circuit partitioning. Given this assumption, the number of required shots will be proportional to the QPD weight, represented by  $\gamma$ .

During the practical application of quantum circuit cutting, which aims to separate an input quantum circuit into independent computation fragments, multiple cuts are often required. A small increase in the single-cut QPD weight, denoted by  $\gamma$ , can lead to a significant increase in the overall cost, both in terms of sampling and quantum resource overhead. SOL is formulated to identify the three cutting scenarios and incorporates the latest optimal theoretical overhead for gate cuts from [48]. For wire cuts, SOL adopts the optimal overhead proposed in [7, 23, 42].

By adopting the optimal overhead, we assume that the associated cutting protocol proposed in previous literature is implemented. However, certain aspects of this protocol are not feasible with current quantum computing platforms, as discussed in [5]. Most notably, QPD should be performed by continuously sampling from the distribution, executing the subcircuit, taking a single measurement, and then sampling again.

Given the scarce availability of quantum computing resources, this sequential process is inefficient. In the current implementation, a fixed number of shots is defined for each subcircuit execution, rather than performing continuous sampling that is expected to be proportional to the QPD weight. As a result, we also present the practical quantum resource overhead for circuit cutting, where the sampling overhead for each cut is not the theoretical optimal value but a fixed value, making the corresponding protocol easier to implement.

For classical cost, given the constraint on the number of qubits available on the hardware, CiFold is optimized to minimize the sampling overhead by maximizing the number of qubits within each subcircuit. This approach is consistent with the objective in [6], which emphasizes optimizing the qubit allocation within subcircuits to reduce overhead.

## 5 Circuit Folding: Modular and Qubit-Level Workload Management

Based on the motivation and problem formulation, we present our system design along with the associated algorithms in this section. First, we develop a graph-based optimization approach that translates a given circuit into a graph representation and generates a workload meta-graph for each individual qubit. Using these graphs, we identify foldable modules within the circuit through a layered pattern discovery method. Finally, these modules are unfolded to maximize their size, optimizing circuit execution and resource usage.

### 5.1 System Overview

Figure 4 presents an overview of the CiFold system. Starting from the left, the system first takes a large circuit as input, which is transformed into a circuit graph consisting of gates and their associated qubit indices. This circuit graph is then further processed and decomposed at the individual qubit level. Each qubit graph represents the complete sequence of gates acting on that specific qubit. Since these gates constitute the computational workload in quantum circuits, the qubit graph also reflects the workload on each qubit.

Next, the qubit-level workload graphs are analyzed to identify frequent patterns across all qubits. Qubits with identical patterns are grouped into foldable modules, with only one copy of each foldable module being recorded, along with its associated qubits and their occurrences. These folded graphs are then unfolded into a single circuit that includes



the repeated modules. Finally, this reassembled circuit is partitioned into smaller subcircuits, allowing it to be executed on existing quantum hardware.

## 5.2 Graph-based Optimization on Recurring pattern

Inspired by the widespread application of graph-based methods in quantum computing, particularly in areas such as compilation [32], we present CiFold—a graph-based approach designed to optimize the circuit folding and reassembly processes. Firstly, the input quantum circuit is transformed into a directed graph  $\mathcal{G} = (V, E)$ , where:

- $V$  is the set of nodes  $v_i$ , and each node corresponds to a gate in the quantum circuit. Each node has attributes: gate type  $g(v_i)$  and qubit index  $q(v_i)$ .
- $E$  is the set of edges connecting the nodes which are potential cutting points. Each edge  $e = (v_i, v_j) \in E$  has the gate name and the weight  $w(e) \in \mathbb{R}_{\geq 0}$ , attributes representing the  $\gamma$ -factor associated with cutting the edge.

The graph  $\mathcal{G}$  encodes the structure of a quantum circuit, with directed wire edges enforcing the correct sequence of gates on each qubit, and bidirectional gate edges representing interactions between qubits. The graph also captures cost of cut individual operation.

To analyze the quantum circuit at the qubit level, we extract a sequence of dependent gates for each qubit  $q_i$ , forming a qubit-level graph  $\mathcal{G}_{q_i}$  as shown in Figure 35. This process can be parallelized by simultaneously parsing the quantum circuit for all qubit indices.

## 5.3 Circuit Folding: Layered Frequent Pattern Discovery

With the graph representation of an input circuit, a qubit-level meta-graph can be constructed to capture its modular structure by folding all nodes and edges with repeated patterns. The pattern graph will provide a simplified and modular representation of the original circuit graph by consolidating these repeated structures. Each node in the meta-graph encapsulates a set of nodes from the circuit graph that share the same gate type, parameters, and intermediate connections to adjacent nodes.

CiFold begins by analyzing the gate sequence at the qubit level. As the example in 5 shows, the nodes of each qubit-level graph represent either gate operating on itself or an entangled qubit. Consequently, every two-qubit gate node is double-counted across all qubit-level graphs. First, most entangled qubit pairs(MEP) will be identified among all qubits. By folding MEP graphs first, we can reduce the number of redundant nodes. The folding algorithm is described in Algorithm 1. It is done in a parallel way such that each pair of graphs can be folded simultaneously. During each layer of folding, the number of individual graphs will be reduced by half and the size of the graph will progressively grow until

the entire circuit is processed. An example of this process is illustrated in Figure 4.

During the folding process, a dynamic programming approach described in Algorithm2 is utilized to find the longest consecutive common subsequence with a default minimum subsequence length of 3. When such a common subsequence is found, the corresponding nodes are folded with a set of folded nodes to keep track of unique nodes in  $G_C$

---

### Algorithm 1 Parallel Folding of Pattern Graphs

---

```

1: Input: Qubit-level Graphs  $\mathcal{G}_{q_0}, \mathcal{G}_{q_1}, \dots$ 
2: Output: Folded graph  $G_{fold}$ 
3: Initialize  $G_{pattern} \leftarrow [\mathcal{G}_{q_0}, \mathcal{G}_{q_1}, \dots]$ 
4: while  $|G_{pattern}| > 1$  do
5:    $MEP(G_{pattern}) \leftarrow [(\mathcal{G}_{q_i}, \mathcal{G}_{q_j}) \mid i \neq j]$   $\triangleright$  Identify merging pairs
6:   for all  $(\mathcal{G}_{q_i}, \mathcal{G}_{q_j}) \in MEP(G_{pattern})$  in parallel do
7:      $[L_i, L_j] \leftarrow LCCS(\mathcal{G}_{q_i}.nodes, \mathcal{G}_{q_j}.nodes, min\_len)$ 
8:     if  $[L_i, L_j] \neq \text{None}$  then
9:        $\mathcal{G}_{q_{i,j}} \leftarrow \text{compose}(\mathcal{G}_{q_i}, \mathcal{G}_{q_j})$ 
10:      for  $(v_i, v_j) \in [L_i, L_j]$ 
11:        Transfer all edges from  $v_j$  to  $v_i$ 
12:         $v_i.join(v_j)$   $\triangleright$  Fold  $v_j$  into  $v_i$ 
13:      Replace  $\mathcal{G}_{q_i}$  and  $\mathcal{G}_{q_j}$  with  $\mathcal{G}_{q_{i,j}}$  in  $G_{pattern}$ 
14:    end if
15:  end for
16: end while
17: return Final pattern graph  $G_{fold}$ 

```

---

## 5.4 Circuit Unfolding: Modular Partitioning Search

The pattern graph from Algorithm 1 is used as a meta-graph to guide the partitioning process, with the aim of leveraging the modular structure within the circuit. This enables simultaneous searching on the circuit graph, knowing that nodes and edges mapped to the same nodes and edges in the pattern graph belong to the same module.

The first step is to find an optimal initial partition. This is achieved using an edge-growth approach described in Algorithm 4 for all folded nodes of the node in the pattern graph with the most folded nodes i.e. nodes in most repeated module. We continue expanding the neighbors of these initial subgraphs until the repeated pattern is disrupted. To avoid the costly structure checks for circuit equivalency, the circuit can be transformed into a graph isomorphism problem.

Two graphs are considered isomorphic if there exists a one-to-one mapping between their nodes such that the connections (edges) between the nodes are preserved. In the context of quantum circuits, an additional consideration is required, ensuring that the node's quantum gate and connection type also match. CiFold employs the Weisfeiler-Lehman (WL) graph hashing technique to efficiently identify isomorphisms. This algorithm encodes the graph's structure

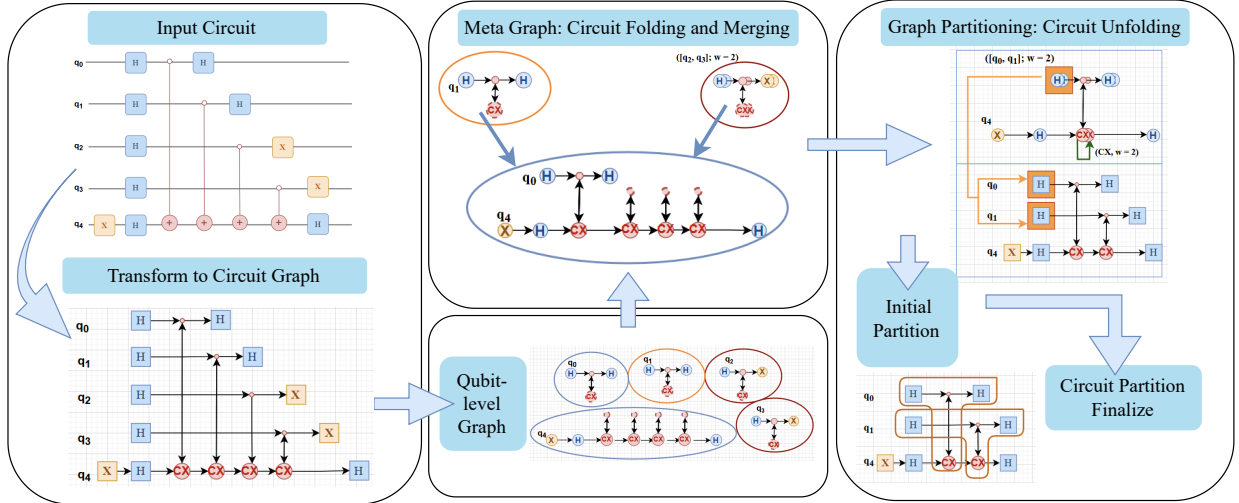


Figure 4. CiFold System Overview

**Algorithm 2** Find Longest Consecutive Common Subsequence

```

1: function LCCS( $S_i, S_j, min\_LCS\_length$ )
2:    $m \leftarrow |seq1|, n \leftarrow |seq2|$ 
3:   Initialize  $dp$  as a table of size  $(m, n)$  filled with 0
4:   Initialize  $max\_len \leftarrow 0$   $\triangleright$  Track the length of the
   longest subsequence
5:   Initialize  $end\_index\_seq1 \leftarrow 0$   $\triangleright$  Track the ending
   index of LCS in  $seq1$ 
6:   for  $i \leftarrow 1$  to  $m$ 
7:     for  $j \leftarrow 1$  to  $n$ 
8:       if  $seq1[i-1] = seq2[j-1]$ 
9:          $dp[i][j] \leftarrow dp[i-1][j-1] + 1$ 
10:        if  $dp[i][j] > max\_len$ 
11:           $max\_len \leftarrow dp[i][j]$ 
12:           $end\_idx\_i, end\_idx\_j \leftarrow i, j$ 
13:        else
14:           $dp[i][j] \leftarrow 0$ 
15:
16:   if  $max\_len \geq min\_LCS\_length$  then
17:     return  $seq1[end\_idx\_i - max\_len : end\_idx\_i]$  :
18:      $seq2[end\_idx\_j - max\_len : end\_idx\_j]$ 
19:   else
20:     return  $\emptyset$   $\triangleright$  Return an empty list
21:   end if
22: end function
    
```

by iteratively refines the node labels of a graph by encoding the graph's structure. Although the WL hash function does not guarantee exact isomorphism, given the additional constraints arising from quantum gate dependencies, it is sufficient for identifying subcircuit equivalency.

**Algorithm 3** Meta-Graph Guided Circuit Partitioning

```

1: Input: Circuit graph  $\mathcal{G}$ , Folded graph  $\mathcal{G}_f$ , qubit constraint  $q_{con}$ 
2: Output: Partitioned subgraphs of the circuit graph
3: Initialize  $VisitedNodes \leftarrow \emptyset$ 
4: Initialize initial partition  $P_{initial} \leftarrow$ 
   ModuleFinding( $\mathcal{G}, \mathcal{G}_f$ )  $\triangleright$  Format:
    $P_{initial}[\text{hash}]: [\text{subgraph}, \dots]$ 
5: Construct a new graph  $G'$  where each initial subgraph
   in  $P_{initial}$  forms a single node
6:  $G' \leftarrow$  Greedy Merge( $q_{con}, P_{initial}$ )
7:  $P \leftarrow$  Refinement( $G', q_{con}, P_{initial}$ )
8: return final partition  $P$ 
    
```

Once the initial partitions are established, they form a supernode by eliminating the internal edges and retaining only the edges between partitions. We then apply a METIS-like graph partitioning algorithm, which performs greedy partitioning to push the size of subcircuits to the qubit constraint limit. Then, the supernodes are deformed, and a refinement process is performed to optimize the execution cost defined in Equation 3, where nodes at the partition boundaries can be exchanged.

## 6 Evaluation

In this section, we evaluated CiFold framework with a range of workloads.

### 6.1 Workload, Implementation and Settings

**Workload:** We evaluate CiFold system with following circuits in different settings. **Adder**[12] circuit is a linear-depth ripple-carry quantum addition circuit that performs addition of quantum states [12]. It facilitates arithmetic operations

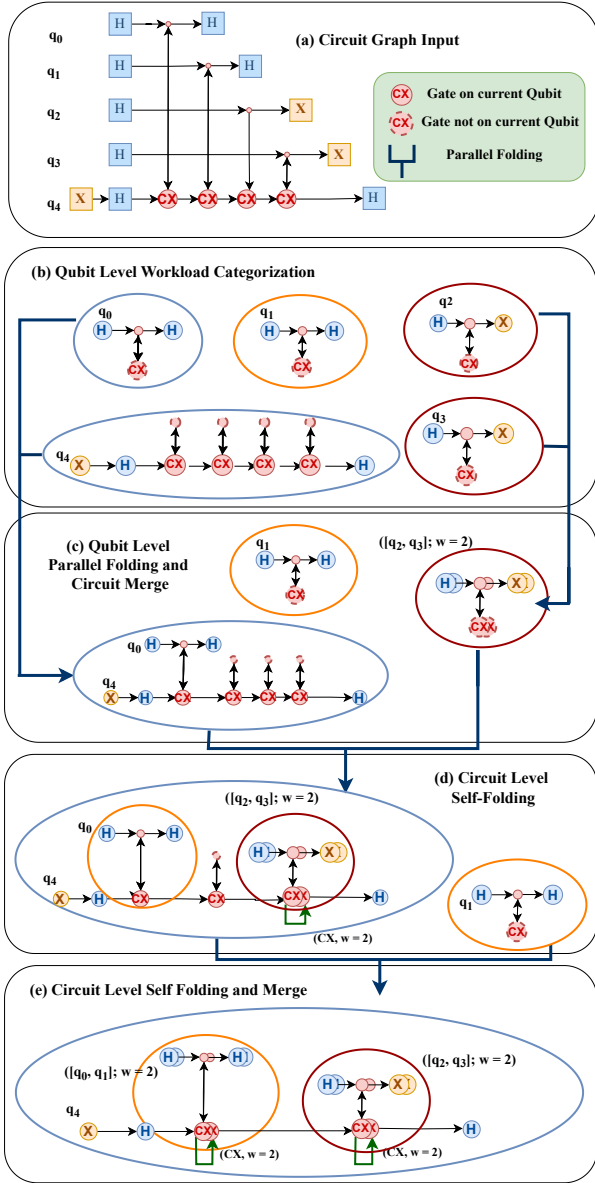


**Figure 5. Illustration of Circuit Folding:** (a) The input quantum circuit is first converted into a circuit-level graph, shown in a, and a qubit-level graph, shown in b. (b) In the first folding layer, the Maximum Entangled Partition identified in b is highlighted using the same color and folded in parallel. (c) During the folding process, a common gate sequence between  $q_2$  and  $q_3$  is detected using the LCCS algorithm (Algorithm 2), resulting in a folded structure with a folding weight ( $w$ ) of 2, as illustrated in c. (d) The folded structure involving  $[q_2, q_3]$  leads to self-folding of  $q_4$ , which is indicated by a green edge pointing towards itself. (e) The final meta-graph exhibits a reduction in nodes (from 19 to 14) and edges (from 18 to 10). The folded nodes in the meta-graph can still be mapped back to the original circuit graph, with each fold indicated by the corresponding  $w$ .

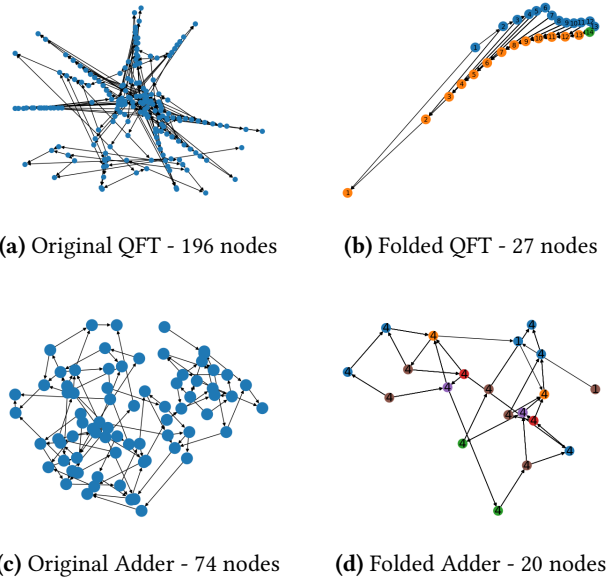


**Figure 6. Comparison of Original Graph and Folded Graph:** Each node in folded graph consolidates multiple nodes in original graph with the number of count indicated. Additionally, nodes of the same color correspond to identical gate types. This folding technique effectively simplifies the large-scale quantum circuit while preserving its key structural characteristics.

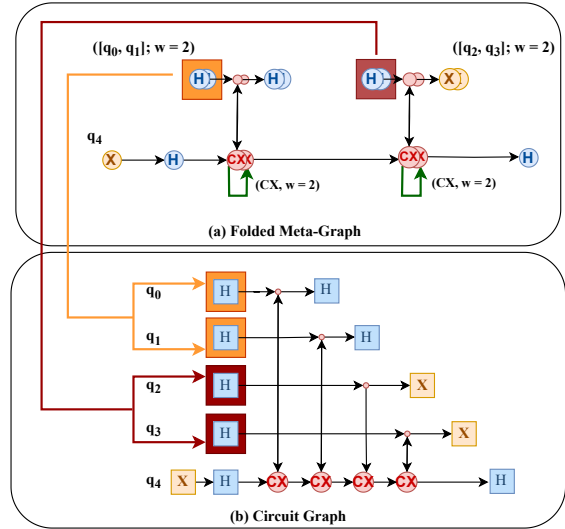


**Figure 7. Illustration of Circuit Unfolding:** The yellow and red arrows pointing from the folded graph in (a) to the circuit graph indicate the unfolding of the folded nodes  $(q_0, q_1), (q_2, q_3)$  in the circuit graph, where edge growth operations are performed simultaneously on these two nodes.

with quantum parallelism and leveraging quantum entanglement. **Bernstein-Vazirani (BV)** circuit solves hidden binary



**Algorithm 4** Optimized Initial Partition with Edge Growth

---

```

1: function MODULEFINDING( $\mathcal{G}, \mathcal{G}_f$ )
2:   Initialize  $visited\_nodes \leftarrow \emptyset$ 
3:   Initialize  $initial\_partition \leftarrow \emptyset$ 
4:   while  $|visited\_nodes| < |\mathcal{G}.nodes|$  do
5:      $v_{freq} \leftarrow \text{Select\_Most\_Folded\_Node}()$ 
6:     Initialize  $best\_subgraph \leftarrow \emptyset, best\_hash \leftarrow \emptyset$ 
7:     for all  $v \in v_{freq}[folded\_nodes]$  in parallel do
8:        $current\_subgraph \leftarrow [v]$  ▷ Initialize
       subgraph with  $v$ 
9:       Identify candidate neighbors of  $v$  in  $\mathcal{G}$ 
10:      for neighbor  $n$  and edge  $e$  connected to  $v$  do
11:        extend edge to  $current\_subgraph$ 
12:      end for
13:       $hash \leftarrow \text{Weisfeiler-Lehman}(current\_subgraph)$ 
14:      select  $best\_subgraph$  based on  $hash$ 
15:       $initial\_partition.append(best\_subgraph)$ 
16:      Update  $visited\_nodes$  with nodes from
        $best\_subgraph$ 
17:    end for
18:  end while
19:  return  $initial\_partition$ 
20: end function

```

---

strings encoded by secret functions using a single query to the black-box oracle, demonstrating quantum advantage of exponential speedup compared with classical methods [4]. **Quantum Fourier Transform (QFT)**[11] is the quantum analog of the classical discrete Fourier transform, used in quantum algorithms to efficiently transform quantum states into the frequency domain, with a diverse applications in phase estimation, factoring (Shor’s algorithm[49]), and solving linear systems of equations. **Greenberger–Horne–Zeilinger (GHZ) state**[19] is a type of entangled quantum state involving three or more qubits, used to demonstrate non-classical correlations and test the principles of quantum mechanics, particularly in applications like quantum communication and quantum cryptography.

**Implementation and Experiment Settings:** We implement the CiFold system with the following software: Python 3.10[45], IBM Qiskit 1.02[1], Qiskit-Addon-Cutting 0.6.0 [5], and Networkx 3.3[21]. The classical components of CiFold are executed on an AMD Ryzen 7 6800H processor running at 3.2 GHz. For the quantum side, we utilize quantum processors from IBM Qiskit Emulators, using fake providers (i.e., noise models derived from real machines): Auckland, Algiers, Toronto, SydneyV2, Peekskill, and Montreal.

To evaluate the accuracy of the reconstructed values, we compare the expected value of the  $Z$ -basis observable for all qubits in the original circuit with the values obtained by executing the subcircuits on the same quantum processing units (QPU) and reconstructing the expected value using

Qiskit-Addon-Cutting. This is a commonly used metric to evaluate a quantum system.

For runtime performance, Quantum Resource Overhead, and practical Quantum Resource Overhead, we compare CiFold with other state-of-the-art circuit cutting techniques in the literature, specifically (1) Qiskit-Addon-Cutting [5] and (2) FitCut [28], using the same input circuits(50-qubit to 190-qubit) on two qubit constraints(20-qubit and 25-qubit).

## 6.2 Observable Value

The quantum circuit cutting technique, upon which we build CiFold cut, is based on quasiprobability decomposition simulation. This approach aims to reconstruct the expected value of a given observable for an  $n$ -qubit quantum system. Let the Pauli string be denoted as  $P$ , which is a tensor product of Pauli operators  $\{I, X, Y, Z\}$  on individual qubits. The expectation value of an observable  $P$  in a state  $|\psi\rangle$  can be expressed as:  $\langle P \rangle = \langle \psi | P | \psi \rangle$ , where  $|\psi\rangle$  is the quantum state of the  $n$ -qubit system. The observable value is a directly measurable quantity in a quantum system and is widely utilized in numerous quantum algorithms. For instance, in quantum chemistry, it represents the energy of a molecule (Hamiltonian). In our study, we implemented circuit cutting using the approach outlined in [5] and conducted experiments on various quantum processors. These experiments were performed using IBM’s noisy emulators, which accurately simulate real-world conditions by replicating the behavior of actual IBM Quantum systems. This was achieved through system snapshots that include crucial details such as the coupling map, basis gates, and qubit properties (e.g.,  $T_1$ ,  $T_2$ , and error rates).

In Figure 8, we present the observable values for a 20-qubit circuit for the BV, Adder, and GHZ circuits. These values are obtained by executing the original circuits, their corresponding subcircuits, and then reconstructing the results. The specified Pauli operator is  $Z^{\otimes 20}$ , and the observable values range from -1 to 1, where the ideal observable value is 1 (i.e., the higher the value, the better). A notable observation is that circuit-cutting techniques significantly improve the observable values in most experiments. For instance, the observable values for the Adder circuit improve as follows: from -0.05 to 0.04, 0.08 to 0.34, -0.04 to 0.00, and -0.01 to 0.07 for the Auckland, Algiers, TorontoV2, and SydneyV2 backends, respectively. These results demonstrate that, under noisy environments, circuit cutting enhances the accuracy of the observable values.

## 6.3 Quantum Resource Overhead

While circuit cutting improves observable values, it suffers from large overhead, as discussed previously. This subsection presents the performance of CiFold in reducing QRO as defined in Equation 3. For each subcircuit, the number of variations to be executed is multiplied by its depth and width. The circuit width represents the number of qubits required

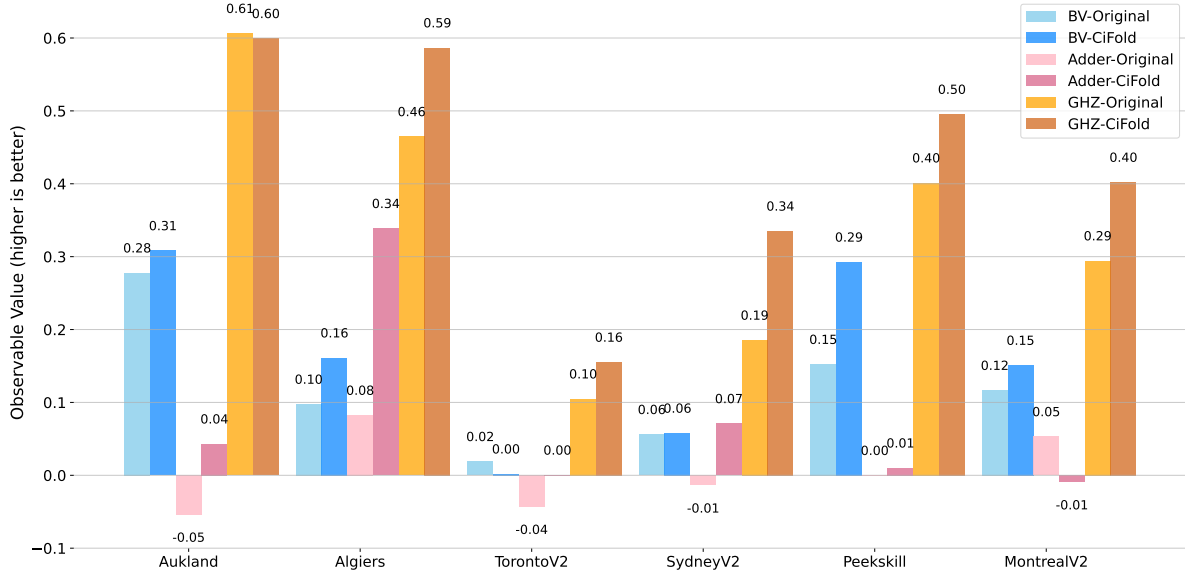


**Figure 8.** Comparison of observable values for BV, Adder, and GHZ circuits with and without circuit cuts.

on the quantum hardware, while the depth corresponds to the number of layers of operations performed in a single execution, with each layer taking approximately constant time to execute. Thus, QRO effectively quantifies the resources demanded from a quantum processor.

A qubit constraint has been fixed for given quantum circuits. The quantum resource overhead presented in Figure 9 effectively measures the cutting quality of CiFold, FitCut, and Qiskit-Addon-Cutting. An interesting observation for the Adder, BV, and GHZ circuits is that the quantum resource overhead closely correlates with their performance on noisy hardware. Specifically, the Adder circuit, which demands the most quantum resources, shows the lowest observable value across all tested QPUs. In contrast, the GHZ circuit, with the least resource requirements, exhibits an observable value closest to the ideal result. Another key distinction of CiFold is its ability to identify both gate and wire connections as potential cutting points, whereas FitCut and Qiskit-Addon-Cutting 0.6.0 are restricted to wire-only cuts. Notably, while latest Qiskit-Addon-Cutting 0.9.0 supports both wire cut and gate cut, due to lack of optimizations, it performs much worse than the previous its version in our experiments and cannot find cut points in most of the evaluations.

Among the four circuit types tested, the QFT circuit demonstrated the highest level of entanglement, leading to a greater number of cuts required to fit within the 20-qubit hardware, which in turn resulted in the highest quantum resource overhead. In Figure 9, we primarily present the result for QFT circuit from CiFold with some missing data points for FitCut and completely missing lines for Qiskit-Addon-Cutting. This is because Qiskit-Addon-Cutting was unable to identify

feasible cutting points within its 300-second API limit. For FitCut, the QRO scaled up to  $10^{14}$ . Given that the quantum volume of publicly available quantum processors typically scales up to 512, applying such a large number of cuts to the QFT circuit with FitCut’s partitioning appears impractical. However, CiFold remained around  $10^7$  and demonstrated stability as the size of the input circuit increased.

For the other three circuit types, CiFold demonstrates stability as the size of the input circuit increases. There are some missing points for Qiskit-Addon-Cutting. Due to its 300-second API limit, it is unable to find feasible cuts in several cases—specifically for the BV circuit when the number of qubits exceeds 90, and for the adder circuit when the number of qubits exceeds 70. Since Qiskit-Addon-Cutting is an exact solver, the presented outcomes are optimal in scenarios where modular structures are not exploited. FitCut also achieves good QRO results; however, its QRO continues to increase with circuit size. In contrast, CiFold maintains a more stable overhead due to the increased number of subcircuits produced as the input circuit grows. For the BV circuit, after the input circuit width exceeds 90 qubits, CiFold shows a significant reduction in QRO, starting from 32.2%, increasing to 64.8%, 100%, 131.6%, and reaching 165.6%. This reduction in QRO is most pronounced for the adder circuit, reaching a maximum of 799.2% for the 190-qubit adder. The GHZ circuit displays a similar trend. When the qubit constraint increases to 25 qubits, the QRO experiences a substantial boost, rising from  $10^1$  to  $10^2$ . Despite this increase, the overall trends for all three methods remain consistent across different settings.

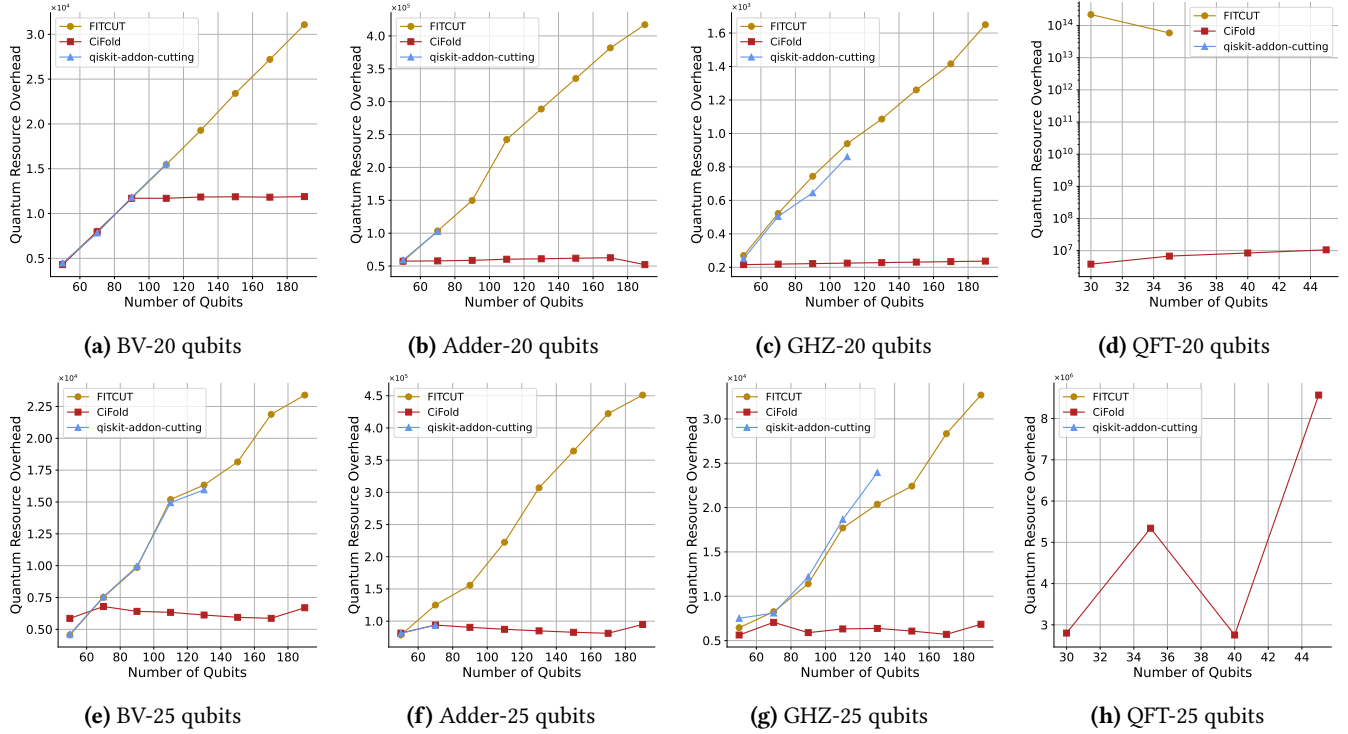


Figure 9. QRO comparison with 20-qubit/25-qubit constraint

#### 6.4 Runtime Performance

The time overhead required to perform circuit partitioning is an important step in the circuit cutting pipeline. Without an automated method to identify cutting points for any given input circuit, it is challenging to establish circuit cutting as a standard protocol in quantum computing. CiFold utilizes a circuit folding technique to reduce the circuit graph complexity to efficiently address this problem. Furthermore, as circuit folding is a parallelized procedure, the time efficiency is significantly improved.

In Figure 10, we present the cut-finding times. Obviously, Qiskit-Addon-Cutting exhibits a consistent trend, with runtimes at approximately 300 seconds for many data points. It arises from an internal 300-second API limit resulting in missing QRO and practical QRO on Figure 9. In contrast, FitCut employs a heuristic approach, achieving very fast runtime. For a 20-qubit constraint, the maximum runtime are 0.21s for the BV circuit, 1.11s for the Adder circuit, and 0.25s for the GHZ circuit. CiFold lies between these two methods, with maximum runtimes of 4.25s for the BV circuit, 7.00s for the Adder circuit, and 3.07s for the GHZ circuit. Its cut-finding times for most cases are under 10 seconds, particularly for structurally simple circuits such as the BV and GHZ circuits. Given the relatively short runtime of CiFold compared to the overall execution and classical post-processing times,

CiFold is efficient enough to be integrated into a circuit-cutting pipeline. Notably, in Figure 10(g), while CiFold appears to perform the worst, the runtime for all three methods is around or below 1 second, making the difference trivial in practical terms.

#### 6.5 Practical Quantum Resource Overhead

Figure 11 presents the QRO using the practical overhead, where the corresponding circuit-cutting technique is directly applicable to current hardware. The missing data points for Qiskit-Addon-Cutting are a result of no feasible solution being returned within the 300-second limit, while for FitCut on the QFT circuit, Figure 11d and Figure 11h, we tested the 30-qubit and 35-qubit with 20-qubit constraint but it yields over  $10^{32}$  which renders implementation infeasible so we didn't perform subsequent experiment. Compared with the theoretical optimal QRO in Figure 9, the  $\gamma$  factor in the QRO (Equation 3) is higher, leading to a rapid increase in QRO as the input circuit size grows.

Under these practical conditions, CiFold demonstrates a more significant reduction in QRO, especially for highly structured circuits where the QRO can remain relatively constant. While a higher  $\gamma$  factor raises this constant, for other methods, the  $\gamma$  factor directly correlates with a steeper increase in QRO as the input circuit size increases. This not only highlights the importance of achieving an optimal  $\gamma$  factor but also suggests that CiFold should be preferred

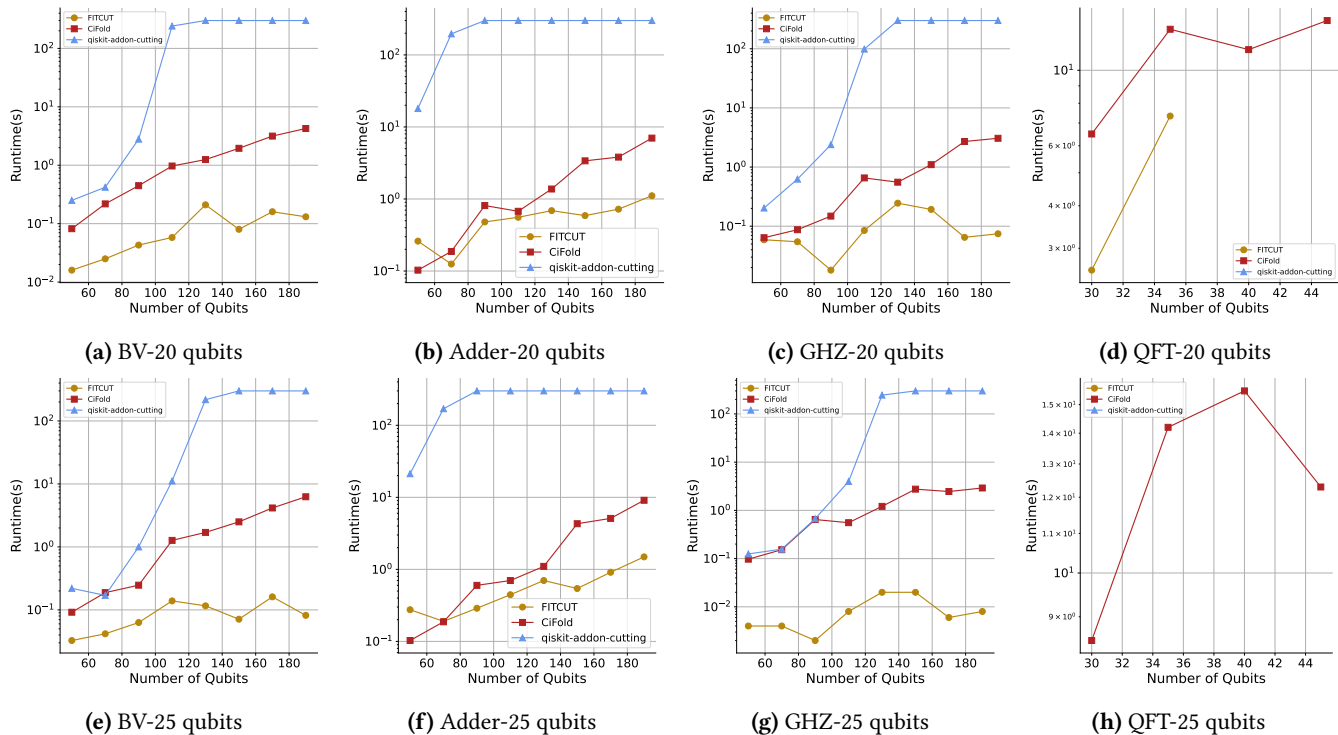


Figure 10. Runtime comparison with 20-qubit/25-qubit constraint

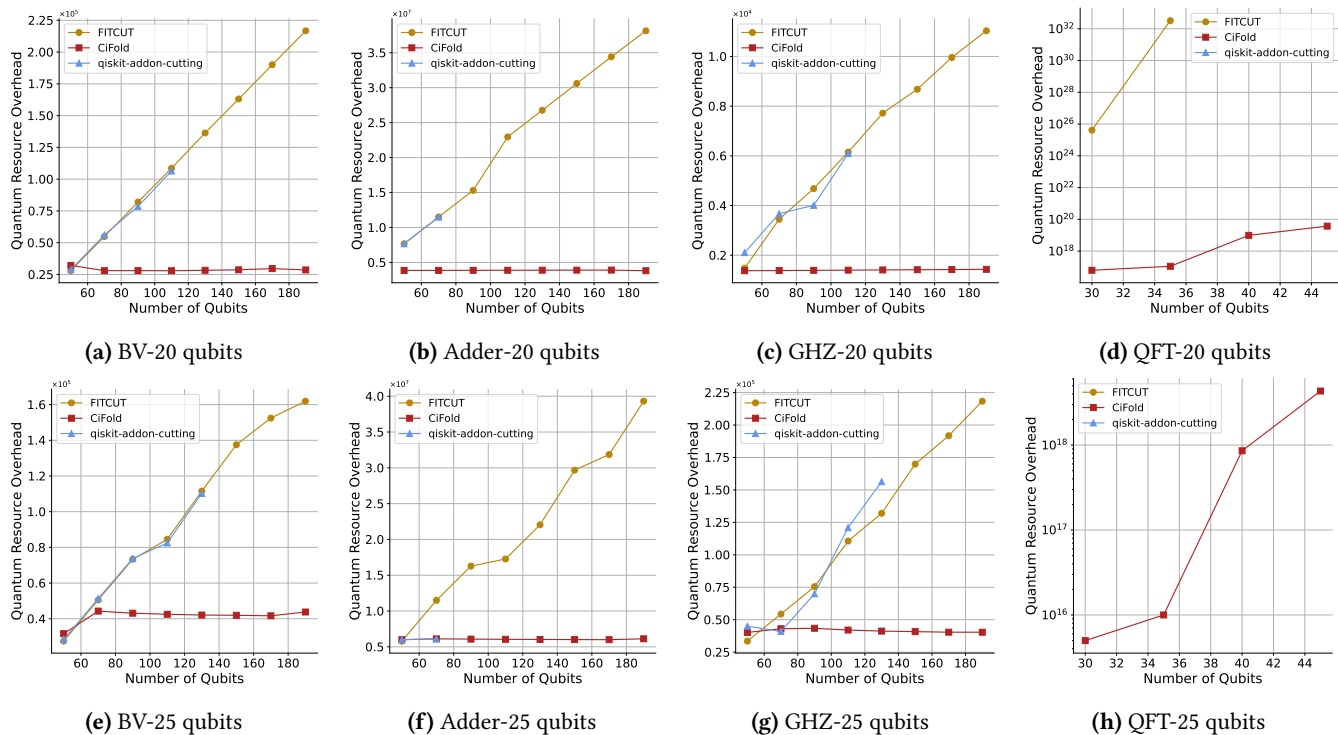


Figure 11. Practical Cost comparison with 20-qubit/25-qubit constraint

when there are constraints or limitations in accessing the latest theoretical advancements. For a 20-qubit constraint, CiFold achieves an average reduction of 5.08 times in practical QRO when tested on 190-qubit circuits, corresponding to reductions of 369% for the Adder circuit, 632% for the BV circuit, and 525% for the GHZ circuit. A similar pattern is observed for test cases with a 25-qubit constraint. This consistent performance indicates that CiFold is well-suited for scenarios requiring efficient circuit-cutting techniques under real-world hardware constraints.

## 7 Conclusion

This paper addresses the problem of circuit cutting in quantum-classical systems. Circuit cutting partitions large quantum circuits into smaller subcircuits that can be executed on noisy, resource-constrained quantum devices. Combined with classical resources, it is a critical technique for advancing quantum computing into practical, commercial applications. However, current approaches suffer from significant overhead, making them infeasible and unscalable. In this paper, we propose CiFold, a graph-based technique that generates qubit-level workloads and identifies foldable modules, i.e., frequent patterns, on individual qubits. CiFold then employs a modular partitioning search algorithm to find the largest repeated modules. Finally, these modules are unfolded to maximize their size, optimizing both circuit execution and resource usage. CiFold is implemented using popular Python libraries and evaluated through extensive experiments in various noisy environments from IBM-Q. The results demonstrate that CiFold improves observable values, significantly reduces quantum resource overhead by up to 799.2%, and maintains fast cutting point identification.

## References

- [1] [n. d.]. IBM Quantum Computing | Qiskit — ibm.com. <https://www.ibm.com/quantum/qiskit>. [Accessed 21-04-2024].
- [2] Betis Baheri, Zixuan Xu, Vipin Chaudhary, Ying Mao, Bo Fang, Shuai Xu, and Qiang Guan. 2022. Pinpointing the system reliability degradation in nisy machines. In *2022 IEEE International Conference on Quantum Computing and Engineering (QCE)*. IEEE, 646–652.
- [3] Marvin Bechtold, Johanna Barzen, Frank Leymann, Alexander Mandl, Julian Obst, Felix Truger, and Benjamin Weder. 2023. Investigating the effect of circuit cutting in QAOA for the MaxCut problem on NISQ devices. *Quantum Science and Technology* 8, 4 (Sept. 2023), 045022. <https://doi.org/10.1088/2058-9565/acf59c>
- [4] Ethan Bernstein and Umesh Vazirani. 1993. Quantum complexity theory. In *Proceedings of the twenty-fifth annual ACM symposium on Theory of computing*. 11–20.
- [5] Agata M. Brańczyk, Almudena Carrera Vazquez, Daniel J. Egger, Bryce Fuller, Julien Gacon, James R. Garrison, Jennifer R. Glick, Caleb Johnson, Saasha Joshi, Edwin Pednault, C. D. Pemmaraju, Pedro Rivero, Ibrahim Shehzad, and Stefan Woerner. 2024. Qiskit add-on: circuit cutting. <https://github.com/Qiskit/qiskit-addon-cutting>. <https://doi.org/10.5281/zenodo.7987997>
- [6] Sebastian Brandhofer, Iliia Polian, and Kevin Krsulich. 2023. Optimal Partitioning of Quantum Circuits Using Gate Cuts and Wire Cuts. *IEEE Transactions on Quantum Engineering* (2023).
- [7] Lukas Brenner, Christophe Piveteau, and David Sutter. 2023. Optimal wire cutting with classical communication. [arXiv:2302.03366 \[quant-ph\]](https://arxiv.org/abs/2302.03366)
- [8] Daniel Chen, Betis Baheri, Vipin Chaudhary, Qiang Guan, Ning Xie, and Shuai Xu. 2022. Approximate quantum circuit reconstruction. In *2022 IEEE International Conference on Quantum Computing and Engineering (QCE)*. IEEE, 509–515.
- [9] Daniel T Chen, Ethan H Hansen, Xinpeng Li, Vinooth Kulkarni, Vipin Chaudhary, Bin Ren, Qiang Guan, Sanmukh Kuppannagari, Ji Liu, and Shuai Xu. 2023. Efficient quantum circuit cutting by neglecting basis elements. In *2023 IEEE International Parallel and Distributed Processing Symposium Workshops (IPDPSW)*. IEEE, 517–523.
- [10] James W Cooley and John W Tukey. 1965. An algorithm for the machine calculation of complex Fourier series. (1965). <https://doi.org/10.1090/s0025-5718-1965-0178586-1>
- [11] James W Cooley and John W Tukey. 1965. An algorithm for the machine calculation of complex Fourier series. *Mathematics of computation* 19, 90 (1965), 297–301. <https://doi.org/10.1090/S0025-5718-1965-0178586-1>
- [12] Steven A Cuccaro, Thomas G Draper, Samuel A Kutin, and David Petrie Moulton. 2004. A new quantum ripple-carry addition circuit. *arXiv preprint quant-ph/0410184* (2004).
- [13] Anthony D’Onofrio, Amir Hossain, Lesther Santana, Naseem Machlovi, Samuel Stein, Jinwei Liu, Ang Li, and Ying Mao. 2023. Distributed quantum learning with co-management in a multi-tenant quantum system. In *2023 IEEE International Conference on Big Data (BigData)*. IEEE, 221–228.
- [14] Suguru Endo, Simon C. Benjamin, and Ying Li. 2018. Practical Quantum Error Mitigation for Near-Future Applications. *Phys. Rev. X* 8 (Jul 2018), 031027. Issue 3. <https://doi.org/10.1103/PhysRevX.8.031027>
- [15] Suguru Endo, Zhenyu Cai, Simon C Benjamin, and Xiao Yuan. 2021. Hybrid quantum-classical algorithms and quantum error mitigation. *Journal of the Physical Society of Japan* 90, 3 (2021), 032001.
- [16] Pascal Friederich, Florian Häse, Jonny Proppe, and Alán Aspuru-Guzik. 2021. Machine-learned potentials for next-generation matter simulations. *Nature Materials* 20, 6 (2021), 750–761.
- [17] Gian Gentinetta, Friederike Metz, and Giuseppe Carleo. 2024. Overhead-constrained circuit knitting for variational quantum dynamics. *Quantum* 8 (2024), 1296.
- [18] Muhammed Golec, Emir Sahin Hatay, Sukhpal Singh Gill, Ying Mao, and Rajkumar Buyya. 2024. Quantum Computing at a Glance. *Authorea Preprints* (2024).
- [19] Daniel M Greenberger, Michael A Horne, and Anton Zeilinger. 1989. Going beyond Bell’s theorem. *Bell’s theorem, quantum theory and conceptions of the universe* (1989), 69–72.
- [20] Lov K Grover. 1996. A fast quantum mechanical algorithm for database search. In *Proceedings of the twenty-eighth annual ACM symposium on Theory of Computing*. 212–219.
- [21] Aric A. Hagberg, Daniel A. Schult, and Pieter J. Swart. 2024. NetworkX: Network Analysis in Python. <https://networkx.github.io/> Version 3.3.
- [22] Tianyi Hao, Kun Liu, and Swamit Tannu. 2023. Enabling high performance debugging for variational quantum algorithms using compressed sensing. In *Proceedings of the 50th Annual International Symposium on Computer Architecture*. 1–13.
- [23] Hiroyuki Harada, Kaito Wada, and Naoki Yamamoto. 2024. Doubly Optimal Parallel Wire Cutting without Ancilla Qubits. *PRX Quantum* 5 (Oct 2024), 040308. Issue 4. <https://doi.org/10.1103/PRXQuantum.5.040308>
- [24] Aram W Harrow and Angus Lowe. 2024. Optimal quantum circuit cuts with application to clustered Hamiltonian simulation. *arXiv preprint arXiv:2403.01018* (2024).
- [25] Sofiene Jerbi, Lukas J Fiderer, Hendrik Poulsen Nautrup, Jonas M Kübler, Hans J Briegel, and Vedran Dunjko. 2023. Quantum machine learning beyond kernel methods. *Nature Communications* 14, 1 (2023),



- 1–8.
- [26] Zihao Jiang, Zefan Du, Shaolun Ruan, Juntao Chen, Yong Wang, Long Cheng, Rajkumar Buyya, and Ying Mao. 2024. Resource-Efficient and Self-Adaptive Quantum Search in a Quantum-Classical Hybrid System. *arXiv preprint arXiv:2405.04490* (2024).
- [27] Matthias Jung, Sven O Krumke, Christof Schroth, Elisabeth Lobe, and Wolfgang Mauere. 2024. QCEDA: Using Quantum Computers for EDA. *arXiv preprint arXiv:2403.12998* (2024).
- [28] Shuwen Kan, Zefan Du, Miguel Palma, Samuel A Stein, Chenxu Liu, Wenqi Wei, Juntao Chen, Ang Li, and Ying Mao. 2024. Scalable Circuit Cutting and Scheduling in a Resource-constrained and Distributed Quantum System. *2024 IEEE Quantum Computing and Engineering (QCE)* (2024).
- [29] Abhinav Kandala, Antonio Mezzacapo, Kristan Temme, Maika Takita, Markus Brink, Jerry M. Chow, and Jay M. Gambetta. 2017. Hardware-efficient variational quantum eigensolver for small molecules and quantum magnets. *Nature* 549, 7671 (Sept. 2017), 242–246. <https://doi.org/10.1038/nature23879>
- [30] Amir H Karamlou, William A Simon, Amara Katarbwa, Travis L Scholten, Borja Peropadre, and Yudong Cao. 2021. Analyzing the performance of variational quantum factoring on a superconducting quantum processor. *npj Quantum Information* 7, 1 (2021), 156.
- [31] Ryan L'Abbate, Anthony D'Onofrio, Samuel Stein, Samuel Yen-Chi Chen, Ang Li, Pin-Yu Chen, Juntao Chen, and Ying Mao. 2024. A Quantum-Classical Collaborative Training Architecture Based on Quantum State Fidelity. *IEEE Transactions on Quantum Engineering* (2024).
- [32] Gushu Li, Yufei Ding, and Yuan Xie. 2019. Tackling the Qubit Mapping Problem for NISQ-Era Quantum Devices. In *Proceedings of the Twenty-Fourth International Conference on Architectural Support for Programming Languages and Operating Systems*. ACM. <https://doi.org/10.1145/3297858.3304023>
- [33] Junde Li, Mahabubul Alam, M Sha Congzhou, Jian Wang, Nikolay V Dokholyan, and Swaroop Ghosh. 2021. Drug discovery approaches using quantum machine learning. In *2021 58th ACM/IEEE Design Automation Conference (DAC)*. IEEE, 1356–1359.
- [34] Junde Li, Rasit O Topaloglu, and Swaroop Ghosh. 2021. Quantum generative models for small molecule drug discovery. *IEEE transactions on quantum engineering* 2 (2021), 1–8.
- [35] Angus Lowe, Matija Medvidović, Anthony Hayes, Lee J O'Riordan, Thomas R Bromley, Juan Miguel Arrazola, and Nathan Killoran. 2023. Fast quantum circuit cutting with randomized measurements. *Quantum* 7 (2023), 934.
- [36] Kosuke Mitarai and Keisuke Fujii. 2021. Constructing a virtual two-qubit gate by sampling single-qubit operations. *New Journal of Physics* 23, 2 (2021), 023021.
- [37] Kosuke Mitarai and Keisuke Fujii. 2021. Constructing a virtual two-qubit gate by sampling single-qubit operations. *New Journal of Physics* 23, 2 (Feb. 2021), 023021. <https://doi.org/10.1088/1367-2630/abd7bc>
- [38] Kosuke Mitarai and Keisuke Fujii. 2021. Overhead for simulating a non-local channel with local channels by quasiprobability sampling. *Quantum* 5 (Jan. 2021), 388. <https://doi.org/10.22331/q-2021-01-28-388>
- [39] Mario Motta, Gavin O Jones, Julia E Rice, Tanvi P Gujarati, Rei Sakuma, Ieva Liepuoniute, Jeannette M Garcia, and Yu-ya Ohnishi. 2023. Quantum chemistry simulation of ground-and excited-state properties of the sulfonium cation on a superconducting quantum processor. *Chemical Science* 14, 11 (2023), 2915–2927.
- [40] Wenrui Mu, Ying Mao, Long Cheng, Qingle Wang, Weiwen Jiang, and Pin-Yu Chen. 2022. Iterative qubits management for quantum index searching in a hybrid system. In *2022 IEEE International Performance, Computing, and Communications Conference (IPCCC)*. IEEE, 283–289.
- [41] Junhong Nie, Qinlin Zhu, Meng Li, and Xiaoming Sun. 2023. Quantum Circuit Design for Integer Multiplication Based on Schönhage-Strassen Algorithm. *IEEE Transactions on Computer-Aided Design of Integrated Circuits and Systems* 42, 12 (2023), 4791–4802.
- [42] Edwin Pednault. 2023. An alternative approach to optimal wire cutting without ancilla qubits. [arXiv:2303.08287 \[quant-ph\]](https://arxiv.org/abs/2303.08287)
- [43] Tianyi Peng, Aram W Harrow, Maris Ozols, and Xiaodi Wu. 2020. Simulating large quantum circuits on a small quantum computer. *Physical review letters* 125, 15 (2020), 150504.
- [44] Christophe Piveteau and David Sutter. 2023. Circuit knitting with classical communication. *IEEE Transactions on Information Theory* (2023).
- [45] Python Software Foundation. 2021. Python Language Reference, version 3.10. <https://www.python.org/>
- [46] Shaolun Ruan, Yong Wang, Weiwen Jiang, Ying Mao, and Qiang Guan. 2022. Vacsen: A visualization approach for noise awareness in quantum computing. *IEEE Transactions on Visualization and Computer Graphics* 29, 1 (2022), 462–472.
- [47] Rei Sato, Kazuhiro Saito, Tetsuro Nikuni, and Shohei Watabe. 2023. Embedding All Feasible Solutions of Traveling Salesman Problem by Divide-and-Conquer Quantum Search. In *2023 IEEE International Conference on Quantum Computing and Engineering (QCE)*, Vol. 2. IEEE, 270–271.
- [48] Lukas Schmitt, Christophe Piveteau, and David Sutter. 2024. Cutting circuits with multiple two-qubit unitaries. [arXiv:2312.11638 \[quant-ph\]](https://arxiv.org/abs/2312.11638)
- [49] Peter W Shor. 1999. Polynomial-time algorithms for prime factorization and discrete logarithms on a quantum computer. *SIAM review* 41, 2 (1999), 303–332.
- [50] Samuel Stein, Ying Mao, James Ang, and Ang Li. 2022. Qucnn: A quantum convolutional neural network with entanglement based backpropagation. In *2022 IEEE/ACM 7th Symposium on Edge Computing (SEC)*. IEEE, 368–374.
- [51] Samuel A. Stein, Betis Baheri, Daniel Chen, Ying Mao, Qiang Guan, Ang Li, Bo Fang, and Shuai Xu. 2021. QuGAN: A Quantum State Fidelity based Generative Adversarial Network. In *2021 IEEE International Conference on Quantum Computing and Engineering (QCE)*. 71–81. <https://doi.org/10.1109/QCE52317.2021.00023>
- [52] Samuel A. Stein, Betis Baheri, Daniel Chen, Ying Mao, Qiang Guan, Ang Li, Shuai Xu, and Caiwen Ding. 2022. QuClass: A Hybrid Deep Neural Network Architecture based on Quantum State Fidelity. In *Proceedings of Machine Learning and Systems*, D. Marculescu, Y. Chi, and C. Wu (Eds.), Vol. 4. 251–264. [https://proceedings.mlsys.org/paper\\_files/paper/2022/file/928f1160e52192e3e0017fb63ab65391-Paper.pdf](https://proceedings.mlsys.org/paper_files/paper/2022/file/928f1160e52192e3e0017fb63ab65391-Paper.pdf)
- [53] Samuel A Stein, Ryan L'Abbate, Wenrui Mu, Yue Liu, Betis Baheri, Ying Mao, Guan Qiang, Ang Li, and Bo Fang. 2021. A hybrid system for learning classical data in quantum states. In *2021 IEEE International Performance, Computing, and Communications Conference (IPCCC)*. IEEE, 1–7.
- [54] Wei Tang, Teague Tomesh, Martin Suchara, Jeffrey Larson, and Margaret Martonosi. 2021. CutQC: using small Quantum computers for large Quantum circuit evaluations. In *Proceedings of the 26th ACM International Conference on Architectural Support for Programming Languages and Operating Systems (ASPLOS '21)*. ACM. <https://doi.org/10.1145/3445814.3446758>
- [55] Kristan Temme, Sergey Bravyi, and Jay M. Gambetta. 2017. Error Mitigation for Short-Depth Quantum Circuits. *Phys. Rev. Lett.* 119 (Nov 2017), 180509. Issue 18. <https://doi.org/10.1103/PhysRevLett.119.180509>
- [56] Barbara M Terhal. 2015. Quantum error correction for quantum memories. *Reviews of Modern Physics* 87, 2 (2015), 307–346.
- [57] Meng Wang, Fei Hua, Chenxu Liu, Nicholas Bauman, Karol Kowalski, Daniel Claudino, Travis Humble, Prashant Nair, and Ang Li. 2023. Enabling scalable vqe simulation on leading hpc systems. In *Proceedings of the SC'23 Workshops of The International Conference on High Performance Computing, Network, Storage, and Analysis*. 1460–1467.

- [58] Dennis Willsch, Madita Willsch, Fengping Jin, Hans De Raedt, and Kristel Michielsen. 2023. Large-scale simulation of Shor's quantum factoring algorithm. *Mathematics* 11, 19 (2023), 4222.
- [59] Lianting Xue, Long Cheng, Yuancheng Li, and Ying Mao. 2021. Quantum machine learning for electricity theft detection: An initial investigation. In *2021 IEEE International Conferences on Internet of Things (iThings) and IEEE Green Computing & Communications (GreenCom) and IEEE Cyber, Physical & Social Computing (CPSCom) and IEEE Smart Data (SmartData) and IEEE Congress on Cybermatics (Cybermatics)*. IEEE, 204–208.
- [60] Kein Yuki Yoshi and Naoki Ishikawa. 2024. Quantum search algorithm for binary constant weight codes. *Quantum Information Processing* 23, 10 (2024), 1–27.
- [61] Maximilian Zinner, Florian Dahlhausen, Philip Boehme, Jan Ehlers, Linn Bieske, and Leonard Fehring. 2021. Quantum computing's potential for drug discovery: Early stage industry dynamics. *Drug Discovery Today* 26, 7 (2021), 1680–1688.